# Electrocatalytic Hydrogenation of Furfural with Improved Activity and Selectivity at the Surface of Structured Copper Electrodes

*Clément Spadetto[1], Cyril Hachemi[1], Maxime Nouaille-Degorce[1], Loïc Pendu[1], Lou Bossert[1], Robert Temperton[2], Andrey Shavorskiy[2], Luis Cardenas[1] and Mathieu S. Prévot*[1]*

[1] Univ. Lyon, Université Claude Bernard Lyon 1, CNRS, IRCELYON, 2 Av. A. Einstein, F-69626 Villeurbanne Cedex, France

[2] MAX IV Laboratory, Lund University, Box 118, 221 00 Lund, Sweden

KEYWORDS: Electrocatalytic hydrogenation, Furfural, Furfuryl alcohol, 2-methylfuran, Selective, High-pressure photoemission, In-situ

https://doi.org/10.26434/chemrxiv-2023-5328j-v2 **ORCID:** https://orcid.org/0000-0003-4367-5502 Content not peer-reviewed by ChemRxiv. **License:** CC BY-NC 4.0

## ABSTRACT

Furfural is a pivotal renewable platform molecule obtained from the chemical breakdown of hemicellulose. While it has traditionally been valorized to value-added chemicals through catalytic hydrogenation in biorefineries, its direct electrocatalytic hydrogenation presents attractive advantages. This article describes the significant improvements brought by the structuring of copper cathodes applied to this process, in terms of activity and selectivity. We show that structured electrodes are capable of converting furfural to furfuryl alcohol with 100% selectivity at potentials as high as - 0.2 V vs. the reversible hydrogen electrode (RHE) in neutral conditions (pH 7.0). Moreover, the same electrode can selectively generate either furfuryl alcohol or 2-methylfuran in acidic conditions (pH 1.0), depending on applied potential and temperature. We further show the existence of optimal voltage-temperature conditions for the efficient conversion of furfural to furfuryl alcohol or 2-methylfuran, highlighting the delicate influence of operating conditions on the selectivity of furfural reduction, in competition with the hydrogen evolution reaction in aqueous electrolytes. These performances are attributed to the resilience of Cu (I) species under operating conditions and their likely contribution to the electrocatalytic active site, as revealed by quasi-in-situ photoelectron spectroscopy.


## INTRODUCTION

The defossilization of the chemical industry requires both to transition away from fossil fuels as a source of energy and to replace petrochemical processes with alternatives based on renewable carbon resources. In this context, the valorization of lignocellulose, the most abundant organic substance on the planet, is of high interest. To achieve its efficient chemical valorization, most



https://doi.org/10.26434/chemrxiv-2023-5328j-v2 **ORCID:** https://orcid.org/0000-0003-4367-5502 Content not peer-reviewed by ChemRxiv. **License:** CC BY-NC 4.0

common biorefinery models are built around a multi-stage scheme involving the separation of lignin, cellulose, and hemicellulose (primary refining), followed by the breakdown of these polymeric compounds into small platform molecules (secondary refining) and finally the chemical upgrading of these platform compounds into value-added chemical feedstock or fuel.[1] Among these platform molecules, furfural (FAL) has been identified as a promising substrate for the production of strategic targets in the value chains of the chemical industry.[2] One attractive way to renewably perform FAL valorization is to use decarbonized electricity to directly power its electrocatalytic reduction, with the advantages of (i) mild temperature and pressure conditions, (ii) the use of water as a source of hydrogen rather than $H_2$, (iii) a potentially more efficient use of renewable electricity compared to electrically heated reactors, and (iv) the possibility of combining FAL reduction with an oxidation process of interest in a single reactor. These concepts can in fact be generalized for the development of electrochemical biorefineries for the sustainable production of fuels and chemicals.[3,4] Regarding FAL electroreduction, two main products are usually identified (see **Figure 1**): furfuryl alcohol (FOH), produced by the reaction of FAL with two protons and two electrons, and 2-methylfuran (2-MF), generated from the reaction of FAL with four electrons and four protons accompanied by the elimination of a water molecule. Finally, a third product is observed for higher concentrations of FAL: the hydrofuroin generated by the reductive coupling of two FAL molecules involving two electrons and two protons (not shown here). This latter product has traditionally been considered as less desirable, although it was recently proposed as a valuable precursor for the development of jet and rocket fuel.[5,6] **Figure 1b** describes the commonly accepted elementary steps involved in the reaction mechanism for the electrocatalytic reduction of FAL.[7] There remains a debate whether these steps occur through an



https://doi.org/10.26434/chemrxiv-2023-5328j-v2 **ORCID:** https://orcid.org/0000-0003-4367-5502 Content not peer-reviewed by ChemRxiv. **License:** CC BY-NC 4.0

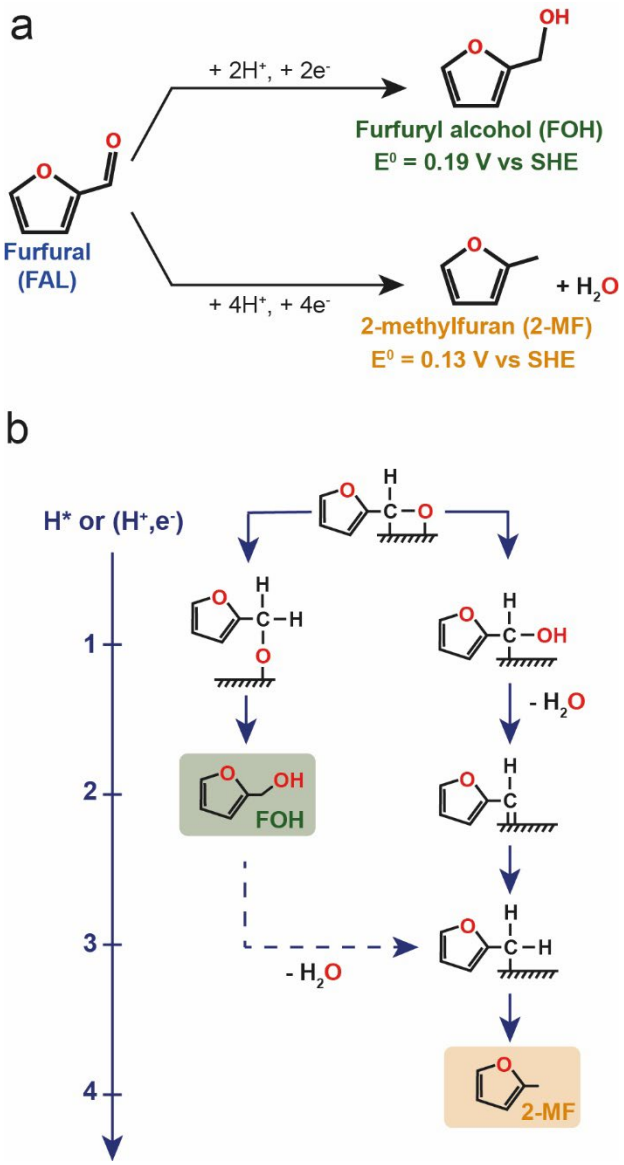


**Figure 1.** a) Electrochemical reduction pathways of furfural into furfuryl alcohol or 2-methylfuran. For each product the corresponding standard reduction potential is reported vs. the standard hydrogen electrode (SHE) from reference 8 where it was calculated from the corresponding Gibbs free energy of formation. b) Corresponding proposed mechanisms involving either the chemical transfer of an adsorbed H (H*) generated by a Volmer step (ECH mechanism) or a proton-coupled electron transfer ($H^+$, $e^-$), or PCET, mechanism. The step corresponding to the dotted arrow, leading to the conversion of FOH to 2-MF is not observed under typical electrocatalytic conditions.

electrochemical hydrogenation (ECH) pathway[9] or through a proton-coupled electron transfer (PCET) pathway.[7] While the first report on the electrocatalytic reduction of FAL dates back to



https://doi.org/10.26434/chemrxiv-2023-5328j-v2 ORCID: https://orcid.org/0000-0003-4367-5502 Content not peer-reviewed by ChemRxiv. License: CC BY-NC 4.0

1939,[10] it has gained a renewed and rapidly growing interest over the last decade and has been the object of several recent perspective and review articles.[11–14] Early studies described the electrochemical reduction of FAL in aqueous media (sometimes containing methanol) inside H-cell setups, on a range of metal electrodes – Pt, Ni, Cu, Al, and stainless steel. [15–18] In more recent studies, Cu has been mostly favored due to its superior activity and selectivity.[9,19–27] These works collectively show that, on bare copper, FAL is selectively converted to FOH under neutral conditions, at applied potentials more negative than - 0.5 V vs. RHE, while 2-MF is the main product under highly acidic conditions at potentials more negative than – 0.45 V vs. RHE (see **Table S3** for a collection of recent data from the literature). In these studies, the concentration of FAL was in the 0.01 – 0.1 M range, with the appearance of hydrofuroin as a secondary product at higher concentrations. Moreover, modifying the copper active site has shown promising improvement in performance. Indeed, employing single-atom copper sites allowed switching from selectively producing FOH at - 0.75 V vs. RHE to selectively producing 2-MF at - 0.9 V vs. RHE in a pH 5 acetate buffer.[24] Moreover, using bimetallic CuPd nanoparticles produced a faradaic efficiency (FE) of 75% for 2-MF in the presence of 0.04 M FAL in 0.1 M acetic acid (pH 2.9) at - 0.58 V vs. RHE, with a 100% selectivity (the remaining FE corresponding to $H_2$ evolution).[25] Similarly, Ni was employed to modulate the electrocatalytic properties of Cu.[27] Finally, a recent study showed the ability of CuO nanowires grown on Cu to reduce FAL to FOH with a much lower overpotential than Cu in 1M phosphate buffer (pH not reported) + 0.05 M FAL.[26] The authors report the selective conversion of FAL to FOH at potentials as high as – 0.2 V vs. RHE, and they attribute this performance to the resilience of some Cu(I) centers to the reductive operating conditions. Finally, it is worth mentioning that some research has been done to successfully implement electrocatalytic reduction of FAL to FOH in flow devices using Pd[8] and



https://doi.org/10.26434/chemrxiv-2023-5328j-v2 **ORCID:** https://orcid.org/0000-0003-4367-5502 Content not peer-reviewed by ChemRxiv. **License:** CC BY-NC 4.0

Cu[28] as cathode materials. Overall, despite significant progress achieved on Cu cathodes for FAL reduction, control over the selectivity of the process remains complicated, as 100% selectivity towards FOH or 2-MF is rarely achieved with the same material, and the potential applied in most studies (- 0.5 to - 0.9 V vs. RHE) indicates the presence of a high overpotential for this electrochemical process. Here, we address these shortcomings and we report the beneficial effects of structuring copper electrodes by a self-templating electrochemical deposition on their performance towards electrocatalytic FAL reduction. We find that, in neutral phosphate buffer (pH 7.0), FAL can be reduced towards FOH with a 100% selectivity at potentials as high as - 0.2 V vs. RHE, representing a significant improvement over the typical potential of - 0.5 V vs. RHE required on Cu electrodes. We further show that, in acidic conditions (pH 1.0) we can direct FAL reduction with 100% selectivity towards either FOH or 2-MF at the surface of the same electrode, depending on the applied potential and the temperature of the electrolyzer. Under all conditions structured electrodes show improved current densities and comparable or better selectivity than polycrystalline copper foil. Surface characterization by UV and X-ray photoelectron spectroscopy, including in-situ measurements performed at the synchrotron, revealed the involvement of Cu(I) species in the electrocatalytic active site, even under reductive operating conditions. Overall, we present an easy and scalable strategy to produce active and selective copper electrodes for the electrocatalytic reduction of FAL towards 2-MF or FOH in aqueous media.



https://doi.org/10.26434/chemrxiv-2023-5328j-v2 **ORCID:** https://orcid.org/0000-0003-4367-5502 Content not peer-reviewed by ChemRxiv. **License:** CC BY-NC 4.0

## METHODS

**Materials.** Furfural (99%, Sigma-Aldrich), furfuryl alcohol (98%, Sigma-aldrich), 2-methylfuran (99% , contains 200-400 BHT as stabilizer), acetonitrile (HPLC-GOLD-Ultragradient grade, Carlo Erba), phosphoric acid (ACS Reagent ≥ 85%, Honeywell), potassium phosphate monobasic (≥ 99.0%, Sigma-Aldrich), potassium phosphate dibasic (ACS Reagant, ≥ 98%, Sigma-Aldrich), copper(II) sulfate pentahydrate (ACS Reagent, ≥ 98%, Sigma Aldrich), and sulfuric acid (ACS Reagant, 95.0-97.0%, Sigma Aldrich) were used without additional purification. An Elga PURELAB Option DV 25 provided the deionised (DI) water (ρ > 18.2 MΩ.cm). A commercial Cu foil (0.25 mm thickness, 99.98% trace metal basis, Sigma-Aldrich) was used as the electrode substrate.

**Cu electrodes preparation.** Cu foil pieces cut to 3x1 $cm^2$ were cleaned thoroughly to remove surface contaminants before testing or electrodeposition. The Cu electrodes were first rinsed with DI water and acetone followed by a 10-min sonication step in acetone and an additional 10 min of sonication in DI water. The Cu foil pieces were dried at room temperature and ready for further electrochemical treatment. Self-templated structured Cu electrodes were produced according to a previously reported methodology.[29,30] Briefly, a current of 1 $A.cm^{-2}$ was applied between two pieces of copper foil immersed in an aqueous solution of 0.4 M $CuSO_4$ + 0.1 M $H_2SO_4$ for different durations using a 2-electrode setup powered by a RS-3005D (RadioSpare) power supply. The deposition time was varied between 10 and 60 seconds. An optimum was found for a deposition time of 40 seconds, corresponding to the maximal development of the porosity of the film, as additional deposited Cu tended to block the pores at longer deposition times (see **Figure S1)**. After electrodeposition, the structured Cu electrodes were carefully rinsed using DI water and soaked for 2 h in DI water to remove unreacted $CuSO_4$. Drying was performed on a hot plate at 60°C for



https://doi.org/10.26434/chemrxiv-2023-5328j-v2 **ORCID:** https://orcid.org/0000-0003-4367-5502 Content not peer-reviewed by ChemRxiv. **License:** CC BY-NC 4.0

18 hours. Epoxy resin was then used to coat the electrode and roughly delimit a 1x1 $cm^2$ active surface area. A small area of pristine copper was left untouched to allow electrical contact with the circuit, but was not exposed to the electrolyte during electrochemical testing. The precise surface area of the electrode was measured each time using the software imageJ.

**Electrochemical setup and experiments.** A commercial air-tight jacketed H-type electrochemical cell (from DekResearch) was used throughout the study. The cell was double-jacketed and a Fisherbrand Polystat was used to control the temperature of the electrolyte. Both compartments of the cell were separated by a proton exchange membrane (Nafion® 117). The anode compartment was filled with 0.1 M potassium phosphate (KPi) buffer or 1 M $H_3PO_4$ for the experiments performed at pH 7.0 and pH 1.0 respectively. FAL was only added to the cathode chamber at a concentration of 0.01 M. All electrochemical experiments were performed with a conventional three-electrode setup connected to a potentiostat (BioLogic SP-300). The Cu working electrodes and the Ag/AgCl reference electrode (3.5 M KCl) were located in the cathode chamber whereas the Pt coil counter electrode was placed into the anode chamber. The potential of the reference electrode is expected to vary by ca. – 20 mV between 20°C and 50°C. When potentials are referenced to the RHE, this shift is partially compensated by the temperature term of the Nernst equation. Overall, the temperature is expected to affect the value of the potential by less than 15 mV in the range of this study. The catholyte was continuously sparged with a 25 $mL.min^{-1}$ $N_2$ flow. This vector gas flowed any volatile and gaseous products through the outlet of the electrochemical cell into a cold trap (-10°C) filled with 15 mL of acetonitrile and cooled by a custom thermostated Peltier device, and sealed with a septum allowing for sampling. Thus, 2-methylfuran was collected in this acetonitrile cold trap, while $H_2$ and $N_2$ were analyzed in real time in a micro-gas chromatograph (INFICON Micro GC Fusion™). During kinetic measurement, the



https://doi.org/10.26434/chemrxiv-2023-5328j-v2 **ORCID:** https://orcid.org/0000-0003-4367-5502 Content not peer-reviewed by ChemRxiv. **License:** CC BY-NC 4.0

gas outlet was detached for less than a minute to collect samples using a syringe. Samples from the cold trap were directly taken through the septum without removing the cap. A scheme and photograph of the setup are provided in **Figure S2**.

**Analysis of products.** NMR experiments were performed by collecting 0.1 mL of electrolyte which was mixed with 0.4 mL $D_2O$ in an NMR tube. Samples were then analyzed in a Bruker 400 MHz NMR spectrometer and data processed in TopSpin 3.6.5. A water peak suppression procedure was applied to each sample (see **Figure S13** for a representative spectrum). HPLC analysis was also performed to analyze liquid products. A Shimadzu High-Performance Liquid Chromatography (HPLC) system equipped with Phenomenex Synergi Hydro-RP column (150 × 4.6 mm) and a Photodiode Array UV-Vis Detector (SPD-M20A) was used. The HPLC analytical condition was set to a column temperature of 30 °C and 1 mL $min^{-1}$ of mobile phase flow rate. Water acquired from an ELGA purelab option-Q purification system in which 0.5 v% $H_3PO_4$ was dissolved (solvent A) and HPLC grade acetonitrile (solvent B) were used as mobile phase solvents. The nonlinear gradient of the two solvents was set to 100% A and 0% B at the start of the experiment and sequentially changed to 99% A and 1% B at 5 min, 80% A and 20% B at 6 min, 10% A and 90% B at 11 min and 100% A and 0% B at 14 min after injection. The total detection duration was 16 min. For a typical measurement, 500 µL of analyte was collected inside in a 2 mL HPLC vial. The results were taken at different wavelengths (210 nm for FAL; 230 nm for 2MF and 232 nm for FOH) by the diode array detector. Identification of analytes was based on the retention time of the HPLC chromatogram while the quantification was done according to calibration curves (see **Figures S11 and S12**) and the ratio of peak areas between analyte and internal standard. HPLC measurement error calculation based on the calibration procedure is detailed in the SI. The $H_2$ production during the tests was quantified using the thermal conductivity



https://doi.org/10.26434/chemrxiv-2023-5328j-v2 **ORCID:** https://orcid.org/0000-0003-4367-5502 Content not peer-reviewed by ChemRxiv. **License:** CC BY-NC 4.0

detector of an INFINICON Micro GC Fusion™. $N_2$ was used as a carrier gas to transport $H_2$ into the micro GC for in-line analysis. The calibration of the system was performed using an electrochemical method: $H_2$ was produced at different current densities on a Pt foil and the quantity of produced $H_2$ was estimated using a 100% FE assumption. The associated measurement error was estimated by averaging three measurements for each current density, and was passed onto FE measurements for $H_2$.

**X-Ray diffraction**. The diffractograms of the electrodes were acquired with a Bruker D8 Advance A25 diffractometer using Cu Kα radiation (□=0.154184 nm). Diffraction angles were scanned between 10 and 80°, and the signal was collected with a one-dimensional multistrip detector (Lynxeye, 192 channels on 2.95°)

**Scanning electron microscopy (SEM).** SEM images were recorded on a Zeiss Merlin Compact, using the secondary electron detector and an acceleration voltage of 5 kV, to document the surface morphology of the prepared electrodes.

**X-Ray Photoelectron Spectroscopy (XPS).** XPS analyses were conducted in an integrated ultrahigh vacuum system, connected to an Axis Ultra DLD spectrometer (Kratos Analytical). Spectra were recorded with a monochromatic Al Kα source (hν=1486.6 eV) operated at a nominal power of 150 W (10 mA x 15 kV). The pass energy was set to 160 eV for wide scans and 40 eV for core levels and Auger lines. The binding energy scale was calibrated with the C 1s of adventitious carbon (284.6 eV). The data were treated using IGOR Pro Software (Wavemetrics Inc.). Peaks were fitted with Voigt functions and a Shirley background. The resolution of the instrument is 0.6 eV.[31] For quasi-in-situ experiments, a portable glove box filled with $N_2$ was used to conduct the electrochemical experiment. The electrochemical cell was installed inside the glove


https://doi.org/10.26434/chemrxiv-2023-5328j-v2 **ORCID:** https://orcid.org/0000-0003-4367-5502 Content not peer-reviewed by ChemRxiv. **License:** CC BY-NC 4.0

box while cables from the potentiostat were introduced through a tight aperture, properly sealed to prevent air leaks inside the glove box. The glove box was under constant $N_2$ flow during the experiment. When the electrochemical test was over, the working electrode was removed from the cell, quickly rinsed and dried on a Kimtech wipe and transferred through an airlock directly from the glove box to the XPS sample chamber, before being put under vacuum and tested. Photographs of the glove-box setup are provided in **Figure S3.**

**In-situ XPS experiment at MAX IV facilities (HIPPIE beamline).** These experiments were carried out at the HIPPIE beamline of the MAX IV Laboratory. Electrochemical experiments were performed using the electrochemical cell available at the beamline, equipped with a three-electrode setup connected to a Bio-Logic SP-200 potentiostat located outside of the instrument. The beamline is equipped with a Scienta HIPP-3 analyzer, with an entrance cone of diameter ~0.15 mm, positioned in the horizontal plane at a 55° angle of the X-ray beam (set to linear-horizontal polarization). An incident photon energy of 1600 eV was used to collect Cu 2p and C 1s spectra and the projected spot size on the sample was ~100x25 $\mu m^2$. The overall photoelectron kinetic energy resolution is estimated to be ~ 0.5 eV. The working electrode was a 2x1 $cm^2$ piece of copper foil, the counter electrode was a Pt wire (diameter 0.3 mm) and the reference electrode was Ag/AgCl/KCl (eDAQ ET072). All three electrodes were held by a manipulator set at the top of the XPS chamber. A beaker containing 1M $H_3PO_4$ (degassed in a separate vacuum chamber prior to use in the XPS instrument) and 0.01 M of furfural when needed, was supported on another manipulator located at the bottom of the chamber. Under operation the equalized chamber pressure was in the 12-15 mbar range after pumping down. For each measurement, a chronoamperometry was performed with all three electrodes immersed in the electrolyte at a given applied potential for 30 min. At the end of the experiment, the electrodes were pulled out of the electrolyte, leaving a


https://doi.org/10.26434/chemrxiv-2023-5328j-v2 **ORCID:** https://orcid.org/0000-0003-4367-5502 Content not peer-reviewed by ChemRxiv. **License:** CC BY-NC 4.0

thin layer of liquid at the surface of the working electrode. This working electrode was then approached to a distance of ~0.3 mm of the analyzer to acquire the XPS data. The electrodes were then immersed again in the electrolyte before proceeding to the next chronoamperometry.

## RESULTS AND DISCUSSION

### Standard characterization

The composition and morphology of the templated electrode was investigated by XRD, XPS and SEM. The XRD data acquired for the electrodeposited copper and for the Cu foil substrate are displayed in **Figure 2a**. The diffractogram of the Cu foil only showed crystalline face-centered cubic Cu(0) with preferential orientation along the {200} range of planes. Conversely, the diffractogram of the structured electrode showed reduced texturing of the Cu(0) phase compared to the pristine foil, and the presence of a $Cu_2O$ phase that did not exhibit strong preferential orientation along any diffraction plane. This indicated that the electrodeposited layer contained randomly oriented Cu(0) and $Cu_2O$ crystals. The morphology of these crystals was then monitored by SEM. **Figure 2b** shows a picture of the typical surface observed for a structured electrode obtained after a deposition time of 40 seconds. A hierarchical architecture was observed: the electrodeposited layer contained microcrystals (in the 100 nm – 1 µm size range) grown around micropores of 10 – 100 µm in diameter. These pores were generated by the concurrent evolution of $H_2$ bubbles during the electrodeposition process. Finally, the chemical compositions of the surface of both the foil and the structured electrode were probed by means of ex-situ XPS. The Cu 2p and Cu LMM signals are displayed in **Figure 2c.** They show that the surface of the copper foil was expectedly mostly composed of Cu(0). This was evidenced by the main Cu 2p peak at 931 eV and the secondary peak at 951 eV in binding energy (BE), stemming from spin-orbit splitting, as



https://doi.org/10.26434/chemrxiv-2023-5328j-v2 ORCID: https://orcid.org/0000-0003-4367-5502 Content not peer-reviewed by ChemRxiv. License: CC BY-NC 4.0

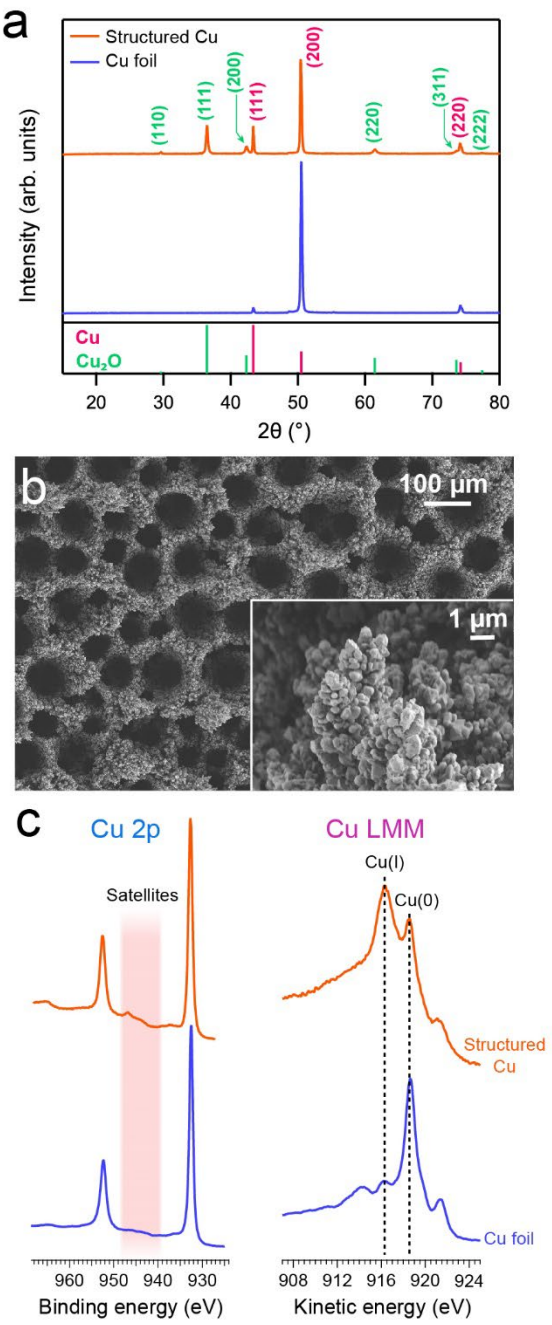


**Figure 2** a) XRD data obtained on the electrodeposited Cu electrode and on the Cu foil substrate. b) Low-magnification SEM picture of the self-templated porous copper electrode Inset: higher magnification SEM picture showing the morphology of electrodeposited Cu microcrystals. c) Cu 2p and Cu LMM XPS spectra measured on bare copper foil and on a structured electrode obtained after 40 seconds of electrodeposition.



https://doi.org/10.26434/chemrxiv-2023-5328j-v2 **ORCID:** https://orcid.org/0000-0003-4367-5502 Content not peer-reviewed by ChemRxiv. **License:** CC BY-NC 4.0

well as by the Auger peak at 918.5 eV in kinetic energy (KE). The presence of faint satellite peaks between 940 and 950 eV in BE in the Cu 2p spectrum and a small Auger peak at 916.5 eV in KE indicated the presence of a small amount of Cu(I) at the surface of the copper foil. In contrast, the XPS spectra of the electrodeposited structured layer show a more pronounced signal for Cu(I) species – satellite peaks in the Cu 2p spectrum and an intense Auger peak at 916.5 eV in KE – revealing that the $Cu_2O$ phase identified by XRD was present at the surface of the freshly structured electrode. Finally, an increase in electrochemical surface area (ECSA) of a factor 15 was found between the bare Cu electrode and the structured one (see **Figure S4** and **S5**).

**Electrochemical conversion of furfural in neutral pH**

The structured copper film was tested as cathode for the reduction of FAL in a three-electrode electrochemical cell (see **Figure S2**). First, cyclic voltammetry (CV) experiments were performed at different temperatures. For each temperature, an iR-corrected CV was acquired on the Cu foil and on the electrodeposited structured Cu electrode. The experiment was first conducted with both the anode and cathode compartments filled with 0.1 M KPi buffer at pH 7.0, and then with the cathode compartment filled with the same 0.1 M KPi buffer to which was added 0.01 M of FAL. This FAL concentration was chosen to prevent the formation of hydrofuroin byproducts, observed at higher concentrations and complicating the study at hand, while providing limited added value to it. In the absence of FAL, the CV of the Cu foil appeared essentially featureless at all temperatures, with a reduction current onset occurring at - 0.5 V vs. RHE, attributed to the HER. On the contrary, the CV of the structured electrode showed an additional reduction wave at all temperatures. This wave was located at - 0.45 V vs. RHE and was attributed to the reduction of Cu(I), coexisting with and prolonged by the HER wave at more negative potentials.[32] The CV scans displayed in **Figure 3a** correspond to a stable measurement over multiple cycles, typically



https://doi.org/10.26434/chemrxiv-2023-5328j-v2 **ORCID:** https://orcid.org/0000-0003-4367-5502 Content not peer-reviewed by ChemRxiv. **License:** CC BY-NC 4.0

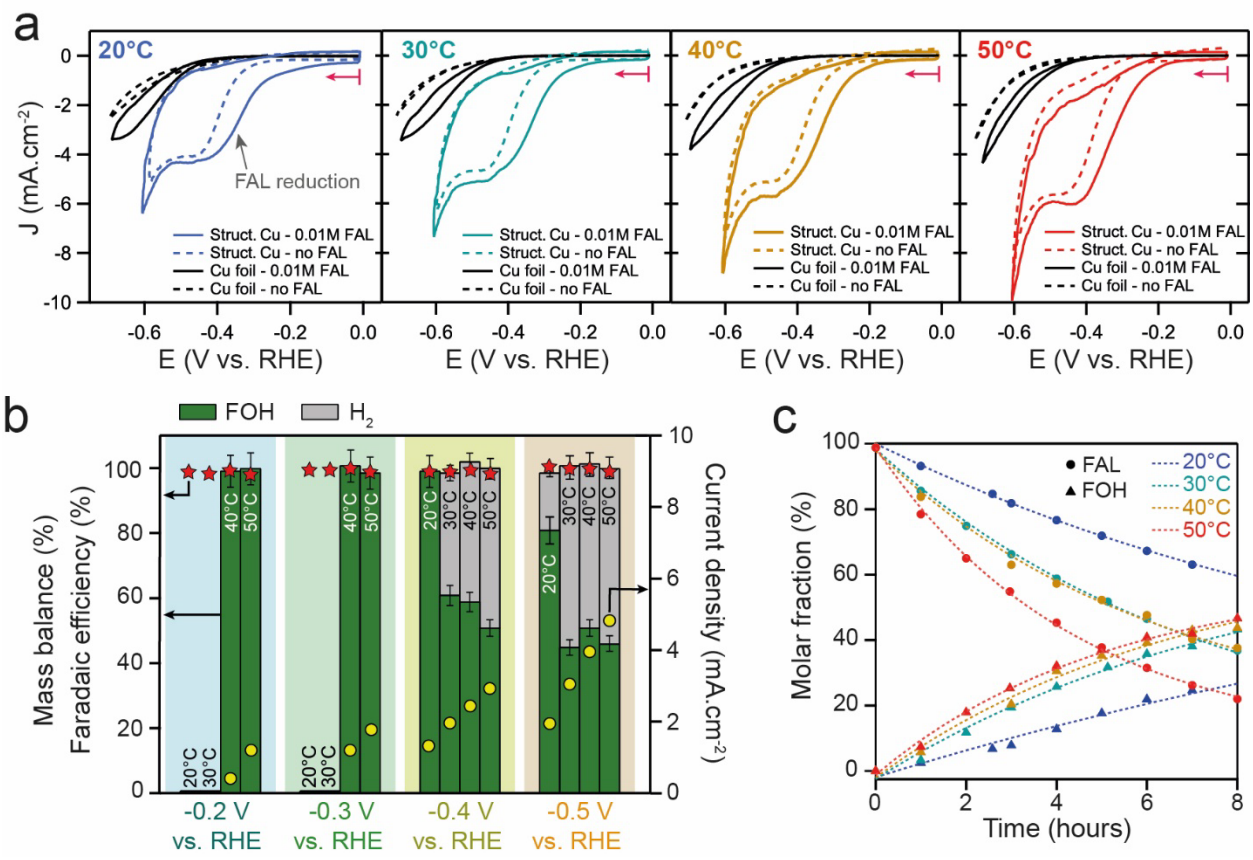


**Figure 3** a) iR-corrected cyclic voltammograms obtained for Cu foil and a structured Cu electrode in the absence (dotted trace) and presence (solid trace) of 0.01 M FAL between 20°C and 50°C. Electrolyte: 0.1 M KPi buffer (pH 7.0). Scan rate: 20 $mV.s^{-1}$ (pink arrow: origin and direction of the scan). b) Values of faradaic efficiencies for $H_2$ and FOH production (bars, left axis) and mass balance (red stars, left axis) measured after 1 hour using structured Cu as working electrode in a 0.1 M KPi + 0.01 M FAL (pH 7.0) between 20°C and 50°C and for applied potentials varying from - 0.2 to - 0.5 V vs. RHE. Yellow markers (right axis) indicate the average current density over the course of the experiment. c) Measured molar fraction of organic compounds collected over time, for an applied potential of - 0.5 V vs. RHE in 0.1M KPi + 0.01 M FAL (pH 7.0) between 20°C and 50°C. The markers represent experimental data, while dotted lines correspond to their fitting with a first-order kinetic model. All measurements performed in under $N_2$ sparging.

obtained after two initial CV scans in which a large quantity of surface oxidized copper is reduced (see **Figure S6**). The fact that the reduction wave at - 0.44 V vs. RHE was part of the stable CV signal indicated that some Cu(I) remained steadily electrochemically accessible in the range of



https://doi.org/10.26434/chemrxiv-2023-5328j-v2 **ORCID:** https://orcid.org/0000-0003-4367-5502 Content not peer-reviewed by ChemRxiv. **License:** CC BY-NC 4.0

monitored potentials. Once FAL was added to the electrolyte, an increase in reduction current was observed both for the Cu foil and the structured Cu. On Cu foil, the reduction current onset was shifted positively by about 50 mV (thus occurring at – 0.45 V vs. RHE) at all temperatures, indicating the kinetically easier reduction of FAL on Cu compared to the HER. This additional reduction current ranging from about – 0.5 to – 1.5 $mA.cm^{-2}$ at - 0.6 V vs. RHE between 20°C and 50°C was associated with FAL reduction on bare Cu foil. On the structured electrode, a slightly larger positive shift in the onset of reductive currents was observed upon FAL addition, accompanied by an increase in current density forming an additional reduction wave. At all temperatures, the onset of this reduction wave was about 0.1 V more positive than the Cu (I) reduction wave onset and merged with it at lower potentials. Because this increase in reduction current was directly linked to the presence of FAL in the electrolyte, it was attributed to the reduction of FAL (indicated by an arrow in **Figure 3a**). Moreover, according to these CV measurements and their proposed interpretation, the onset of FAL reduction on structured Cu electrodes was measured at ca. - 0.15 V vs. RHE. To confirm the ability of structured Cu to reduce FAL at such low overpotentials and to study the selectivity of the process, chronoamperometry (CA) measurements coupled with product identification and quantification were performed at several potentials (- 0.2, - 0.3, - 0.4 and - 0.5 V vs. RHE) and temperatures (20°C, 30°C, 40°C and 50°C). The results obtained after 1 hour of CA under each condition are presented in **Figure 3b**. No product was detected after one hour at - 0.2 and - 0.3 V vs. RHE at 20°C and 30°C. On the contrary, when the temperature was raised to 40°C and above, FOH was generated with an FE of 100%. Furthermore, FOH could also be generated with a 100% FE at - 0.4 V vs. RHE at 20°C. Higher temperatures and more negative potentials resulted in the apparition of $H_2$ as a competing reduction product from HER. Under all conditions, FOH was selectively produced from the



https://doi.org/10.26434/chemrxiv-2023-5328j-v2 **ORCID:** https://orcid.org/0000-0003-4367-5502 Content not peer-reviewed by ChemRxiv. **License:** CC BY-NC 4.0

reduction of FAL as no other product was detected by NMR, HPLC or micro-GC, and a mass balance above 95% was consistently measured. Interestingly, when the same experiment was performed on Cu foil, negligible current densities and no FAL conversion were measured after 1 hour of polarization at - 0.5 V vs. RHE (see **Table S1**), highlighting the significantly improved electrocatalytic properties of structured Cu electrodes compared to the performance of Cu foil: we show that our structured Cu electrodes can selectively convert FAL to FOH with a 100% FE at minimal overpotential. Furthermore, SEM analysis of our structured Cu electrode after 2 hours of operation at – 0.5 V vs. RHE showed no evident alteration of the morphology compared to its initial state (see **Figure S8**). While little data on FAL reduction on Cu at pH 7 is available in the literature, this result represents an improvement over a 98% FE for FOH reported on Cu single atoms at – 0.75 V vs. RHE in acetate buffer (pH 5.0),[24] or to a 70 - 85 % FE for FOH reported on CuO nanowires for potentials between - 0.2 and - 0.3 V vs. RHE in phosphate buffer (unspecified pH).[26] To investigate the kinetics of the process, FAL reduction was conducted on structured Cu electrodes at - 0.5 V vs. RHE and at 20°C, 30°C, 40°C and 50°C. The results of this experiment are shown in **Figure 3c**. Over the course of the experiment, no other FAL reduction product than FOH was detected. The conversion of FAL to FOH was found to follow an apparent first-order kinetic law at all temperatures, with a typical increase in the rate of reaction with the temperature. However, as the temperature was increased, increasingly noticeable amounts of FAL evaporated from the electrolyte over time, carried away by the sparging $N_2$ flow and was captured in the cold trap. After 8 hours of experiment, 9% of unreacted FAL escaped the reactor at 20°C, while up to 25% of it escaped the reactor at 50°C. This explains the difference in apparent rate between FAL disappearance from the electrolyte and FOH production at 50°C in **Figure 3f**. When fitted with the Arrhenius equation, the kinetic data obtained for FOH production afforded an apparent


https://doi.org/10.26434/chemrxiv-2023-5328j-v2 **ORCID:** https://orcid.org/0000-0003-4367-5502 Content not peer-reviewed by ChemRxiv. **License:** CC BY-NC 4.0

activation energy of 23 kJ.mol$^{-1}$ (see **Figure S7**). This value was found comparable to what others measured for catalytic aldehyde hydrogenation towards alcohol in thermochemical or electrochemical setups.[33–37] However, considering the experimental setup employed in this study (unstirred batch H-cell and low FAL concentration), we posit that diffusion kinetics are limiting. This was supported by the fact that stirring the electrolyte resulted in an increase in current density (see **Figure S7**) both in the presence and absence of FAL due to the poor ionic conductivity of the 0.1 M KPi electrolyte. Still, the increase in current was observed to be larger in the presence of FAL, suggesting mass transport limitations. Overall, these experimental results prove that FAL can be selectively converted to FOH at much improved overpotential on the surface of structured Cu electrodes under neutral conditions and at temperatures below 50°C.

**Electrochemical conversion of furfural in acidic pH**

It is well known that pH has a strong influence on FAL reduction selectivity at the surface of copper, with an increased selectivity towards 2-MF over FAL at low pH.[10] While most studies have been conducted in $H_2SO_4$ electrolytes (see **Table S3**), we chose to employ $H_3PO_4$ as a source of protons, so as to keep the same counter anion ($PO_4^{3-}$) as in our study in neutral conditions (in which the electrolyte was buffered with potassium phosphate salts). Thus, the following experiments were conducted in a 1M $H_3PO_4$ solution exhibiting a pH of 1.0. First, iR-corrected CV were collected for Cu foil and structured Cu electrodes at 20°C, 30°C, 40°C and 50°C in the absence and presence of 0.01M FAL. The resulting curves are shown in **Figure 4a**. They revealed that, in acidic conditions, both Cu foil and structured Cu generated much higher current densities



https://doi.org/10.26434/chemrxiv-2023-5328j-v2 **ORCID:** https://orcid.org/0000-0003-4367-5502 Content not peer-reviewed by ChemRxiv. **License:** CC BY-NC 4.0

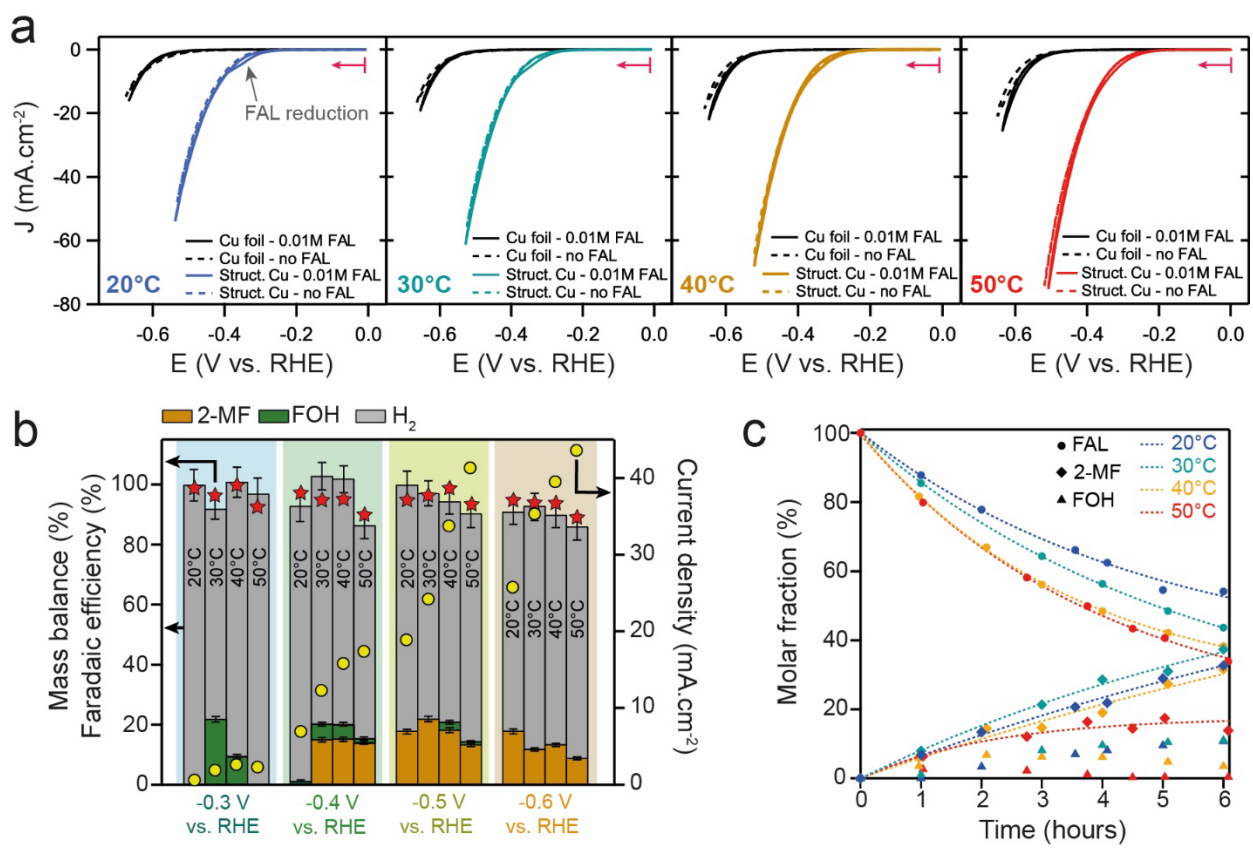


**Figure 4** a) iR-corrected cyclic voltammograms obtained for Cu foil and a structured Cu electrode in the absence (dotted trace) and presence (solid trace) of 0.01 M FAL between 20°C and 50°C. Electrolyte: 1 M $H_3PO_4$ (pH 1.0). Scan rate: 20 $mV.s^{-1}$ (pink arrow: origin and direction of the scan). b) Values of faradaic efficiencies for $H_2$, FOH, and 2-MF production (bars, left axis) and mass balance (red stars, left axis) measured after 1 hour using structured Cu as working electrode in a 1 M $H_3PO_4$ + 0.01 M FAL (pH 1.0) between 20°C and 50°C and for applied potentials varying from - 0.2 to - 0.5 V vs. RHE. Yellow markers (right axis) indicate the average current density over the course of the experiment. c) Measured molar fraction of dissolved organic compounds in the electrolyte and in the cold trap over time, for an applied potential of - 0.5 V vs. RHE in 1M $H_3PO_4$ + 0.01 M FAL (pH 1.0) between 20°C and 50°C. The markers represent experimental data, while dotted lines correspond to their fitting with a first-order kinetic model (only for FAL and 2-MF). All measurement performed under $N_2$ sparging

that in neutral pH, indicating a drastic promotion of HER on Cu electrodes at low pH. Interestingly, while the onset of HER was observed at - 0.50 V vs. RHE on Cu foil, it shifted to - 0.30 V vs.



https://doi.org/10.26434/chemrxiv-2023-5328j-v2 ORCID: https://orcid.org/0000-0003-4367-5502 Content not peer-reviewed by ChemRxiv. License: CC BY-NC 4.0

RHE on the structured electrode, showing significantly enhanced electrocatalytic HER activity. Moreover, contrary to what was observed in neutral conditions, no defined feature was observed in the CV of either the Cu foil or the structured Cu. This suggested that once reduced over the first CV scan (see **Figure S6**), the surface oxide layer was not electro-active in this range of potentials. When FAL was introduced in the electrolyte, a slight positive shift of a few tens of mV in onset potential was observed on Cu foil at all temperatures. On the structured electrodes, the introduction of FAL also resulted in a minor shift in onset potential, accompanied by the appearance of a reduction wave located at the foot of the HER wave. This reduction wave, located roughly between - 0.30 and - 0.35 V vs. RHE at all temperatures was thus attributed to FAL reduction (indicated by an arrow in **Figure 4a**). Moreover, as the temperature increased, this FAL reduction wave was increasingly merged with the HER wave, suggesting a different influence of temperature on the reduction kinetics of water and FAL in 1M $H_3PO_4$. Contrary to what was observed under neutral conditions, and similarly to what occurred on the Cu foil, there was little change in electrochemical activity upon addition of FAL, indicating a stronger competition between the HER and FAL reduction. Again, 1-hour CA experiments were performed at - 0.3, - 0.4, - 0.5 and - 0.6 V vs. RHE, each at 20°C, 30°C, 40°C and 50°C in 1M $H_3PO_4$ + 0.01 M FAL on the Cu foil and on the structured electrode. Importantly, 2-MF, because of its low solubility in water and relatively high volatility, rapidly exited the electrochemical cell, carried away by the $N_2$ stream (something that was not observed with FOH), justifying the use of a cold trap. 2-MF was recovered in this trap and quantified by HPLC measurements, whereas FOH was collected and measured inside the working electrode compartment (similar to under neutral conditions). Finally, $H_2$ evolution was quantified by a micro-GC connected in-line with the outlet of the cold trap (see **Figure S2**). For all measurements, a total FE in the 87 - 106 % range was obtained. Lower FE values were typically



https://doi.org/10.26434/chemrxiv-2023-5328j-v2 **ORCID:** https://orcid.org/0000-0003-4367-5502 Content not peer-reviewed by ChemRxiv. **License:** CC BY-NC 4.0

obtained at high temperature, and were correlated to lower mass balance values (**see Figure 3b**). Besides failure of trapping all products in the cold trap, a possible reason for these lower values can be the existence of homogeneous side-reactions leading to the degradation of furanic compounds in acidic conditions. These side reactions have been well documented by others, especially at higher FAL concentration and have resulted in low mass balance values in the past.[13,20,21]The FE measured on the structured Cu after each CA are displayed in **Figure 4b**. At - 0.2 V vs. RHE, at all temperatures, very low current densities (below 0.1 $mA.cm^{-2}$, not shown in **Figure 4b**) were measured and only traces amount of $H_2$ were detected, in contrast with what was observed in neutral conditions. When the potential of the working electrode was shifted to - 0.3 V vs. RHE at 20°C, similarly low current densities were measured and only $H_2$ was detected as a product. However, FAL conversion was observed to be selective towards FOH at 30°C and 40°C. Further increasing the temperature from 30°C to 40°C at this potential led to an increase in $H_2$ production, but did not affect the selectivity of FAL reduction, which remained 100% directed towards FOH. Interestingly, increasing the temperature to 50°C further favored the HER to the point of preventing FAL reduction altogether. This indicated that, at - 0.3 V vs. RHE, increasing the temperature improved the kinetics of both FAL reduction and HER, but that the HER was kinetically more favored at high temperature. This resulted in an optimum for FAL reduction at around 30°C. When subjected to - 0.4 V vs. RHE, the structured Cu was once again capable of reducing FAL only at temperatures above 30°C, despite significant current densities drawn at 20°C, showing that HER proceeded more easily than FAL reduction at this temperature. However, at this potential and above 30°C, the selectivity of FAL reduction was preferentially directed towards 2-MF, although a significant amount of FOH was also detected as secondary product. Once again, when the temperature was raised from 30 to 40 and finally 50°C, FAL reduction was


https://doi.org/10.26434/chemrxiv-2023-5328j-v2 **ORCID:** https://orcid.org/0000-0003-4367-5502 Content not peer-reviewed by ChemRxiv. **License:** CC BY-NC 4.0

increasingly more disfavored compared to HER. However, the FE towards 2-MF was not affected and remained quasi-constant at around 15%, indicating that temperature affected both reduction pathways differently. Indeed, at - 0.4 V vs. RHE, the increase in $H_2$ production was exclusively achieved to the detriment of FOH production (similarly to what was observed at - 0.3 V vs. RHE). Finally, at - 0.5 V vs. RHE, a much better selectivity for 2-MF was achieved, since a conversion of FAL with a 100% selectivity towards 2-MF was observed at 20°C and 30°C, while only a few percent of FOH were detected at higher temperature. At this potential, an optimal activity for 2-MF production was measured at 30°C, where a FE of 22% was obtained for 2-MF and no FOH was detected. When subjected to the same conditions, Cu foil only produced very small current densities, making the accurate quantification of products and the calculations of FE difficult with our experimental setup, although we can report that only 2-MF and $H_2$ were detected as products (see **Table S2**). Previous studies similarly showed that, on Cu foil and in acidic conditions, at low FAL concentration (0.01 – 0.02 M), $H_2$ was the major product in the reduction range of FAL.[9,21] In these studies, the selectivity towards 2-MF could be improved by increasing FAL concentration, but to the detriment of the overall mass balance, suffering from aforementioned homogeneous degradation reactions. We show here that structuring Cu by our approach does not provide a satisfying answer to the competition of HER, as both FAL reduction and HER were enhanced by the structuration of the electrocatalyst. Kinetics measurements were then performed at - 0.5 V vs. RHE for temperatures of 20°C, 30°C and 40°C and the results are presented in **Figure 4c**. As expected, an increased rate of FAL reduction was measured with increasing temperature. Once again 15 to 30% (at 20°C and 50°C respectively) of initial FAL was measured to evaporate and leave the reactor over the course of the experiment. Furthermore, it appeared that, contrary to what the data presented in **Figure 4b** and collected after only one hour may suggest, FOH was ultimately



https://doi.org/10.26434/chemrxiv-2023-5328j-v2 **ORCID:** https://orcid.org/0000-0003-4367-5502 Content not peer-reviewed by ChemRxiv. **License:** CC BY-NC 4.0

produced at all temperatures, but with a temporal delay compared to 2-MF. This indicated a change in the environment of the electrocatalytic site over time. We rationalize this behavior by suggesting that as HER and FAL proceed at the surface of the electrode, the consumption of protons shifts the local pH towards higher values, in turn shifting the selectivity of FAL reduction towards FOH production. This is consistent with the observation that FOH production occurs sooner at higher temperatures, at which higher current densities indicate faster proton consumption and therefore faster increase in the local pH. Finally, we observe that the concentration of generated FOH decreases over time, indicating chemical degradation of this compound in acidic media. This was confirmed by NMR analysis, revealing that the furanic ring underwent an opening, leading to the formation of a non-identified non-aromatic degradation product (see **Figure S12**). Furthermore, attempts at calculating the apparent activation energy of the process based on the kinetics of 2-MF production resulted in a non-Arrhenius behavior (see **Figure S10**). This uncharacteristic dependence on temperature can be linked to an array of experimental hurdles with our setup: the need to collect 2-MF in a separated cold trap with unclear transfer kinetics (e.g. condensation in the transfer line), the aforementioned existence of homogeneous degradation of furanic compounds in acidic conditions, and the existence of mass transport limitations. Indeed, similar to what was observed under neutral conditions, increase in current upon stirring suggested that mass transport was also limiting in our experiment (see **Figure S7b**) in acidic conditions. It is however worth noting that others have successfully estimated an apparent activation energy for 2-MF production in acidic conditions based on initial rate analysis, rather than fitting of data over the course of several hours.[37] Finally, SEM analysis showed no significant change in the surface morphology of structured copper after operating in acidic conditions (see **Figure S8**). Overall, the results presented in **Figure 4** demonstrate the possibility to tune the selectivity of FAL reduction



https://doi.org/10.26434/chemrxiv-2023-5328j-v2 **ORCID:** https://orcid.org/0000-0003-4367-5502 Content not peer-reviewed by ChemRxiv. **License:** CC BY-NC 4.0

as a function of applied potential and temperature, and show that the selectivity of the process is highly sensitive to the local environment of the active site. We believe in particular that the local pH can quickly change under operating conditions, resulting in shifts in selectivity over time. Despite the preponderance of the HER under the conditions of this study, we demonstrated that FAL could be converted in 1M $H_3PO_4$ at potentials as high as - 0.3 V vs. RHE and achieve complete initial selectivity towards FOH at -0.3 V vs. RHE (although the product quickly degrades) and towards 2-MF at - 0.4 V vs. RHE and below. To better illustrates the latter, **Figure 5** represents the evolution of different metrics as a function of applied potential and temperature measured after 1 hour of FAL reduction in 1 M $H_3PO_4$. The contour plots represented in this figure were obtained by interpolating experimental values measured on the location of each marker (16 data points for each plot). **Figure 5a** shows that there is an optimal combination of temperature and applied potential to promote the conversion of FAL in our setup, namely 40°C and - 0.5 V vs. RHE. Indeed, at more positive voltages and lower temperature, lower current densities resulted in lower conversion rate, while at more negative voltage and higher temperature, HER was increasingly favored over FAL reduction. Moreover, **Figure 5b** shows the existence of two regimes of selectivity, mostly determined by the applied voltage: at potentials more positive than - 0.35 V vs. RHE, FOH was the main product of FAL, while at potentials more negative to this value, 2-MF was the major product. Importantly, it was found that both products could be selectively obtained in appropriately chosen temperature/voltage domains, although FOH was found to degrade over time in acidic conditions. This was confirmed with the measurement of FE for both products, pictured in **Figure 5c-d**. These plots further show that a temperature-voltage optimum exists for 2-MF production, as a result of the optimum in conversion rate and selectivity discussed previously.



https://doi.org/10.26434/chemrxiv-2023-5328j-v2 **ORCID:** https://orcid.org/0000-0003-4367-5502 Content not peer-reviewed by ChemRxiv. **License:** CC BY-NC 4.0

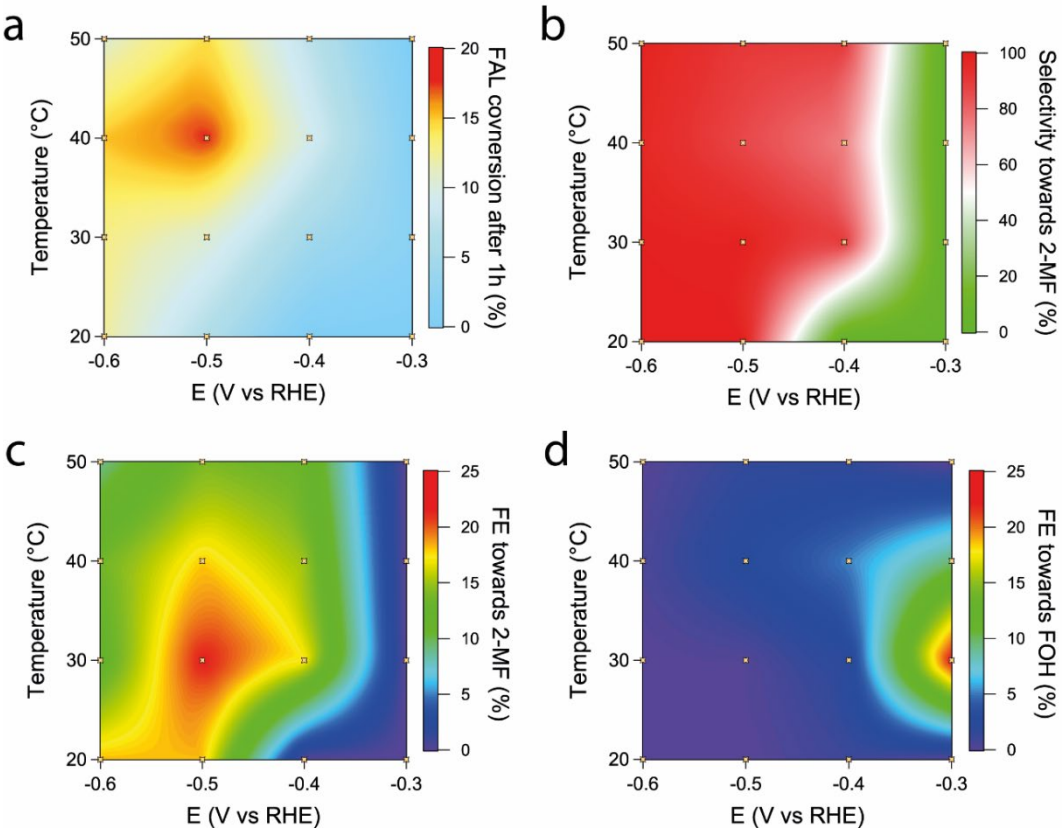


**Figure 5** Contour plots of (a) the conversion of FAL, (b) the selectivity of FAL reduction towards 2-MF, the only other conversion product being FOH, (c) the Faradaic efficiency towards FOH production and (d) the Faradaic efficiency towards 2-MF production, as a function of temperature and applied voltage after 1 hour of electrolysis at the surface of a structured Cu electrode in 1 M $H_3PO_4$ in our electrochemical cell. Markers indicate the experimental data used to plot the figures.

**Photoelectron spectroscopy analysis**

To understand the difference in activity and selectivity between our structured electrodeposited copper electrode and the copper foil, we relied on photoelectron spectroscopy. First, quasi-in- situ XPS experiments were performed in our laboratory. A structured electrode was subjected to electrolysis conditions (in neutral or acidic electrolyte) in the presence of FAL for 30 min at - 0.5 V vs. RHE, and quickly transferred under inert atmosphere to the XPS chamber for analysis (see Methods section). The acquired Cu 2p and Cu LMM spectra are shown in **Figure 6a**. The spectral



https://doi.org/10.26434/chemrxiv-2023-5328j-v2 **ORCID:** https://orcid.org/0000-0003-4367-5502 Content not peer-reviewed by ChemRxiv. **License:** CC BY-NC 4.0

signature of Cu(I) – satellites peaks and shoulder at 934 eV in the Cu 2p spectrum and the peak at 916.5 eV in KE in the Cu LMM spectrum – revealed that surface Cu(I) existed under operating conditions at both pH. The corresponding C 1s spectra are displayed in **Figure 6b**, exhibiting several peaks indicating the presence of different carbon species at the surface of the electrode. Under acidic conditions, the main peak at 284.6 eV was attributed to C-C and C-H bonds, while the smaller peak at 286.1 eV was attributed to C-O bonds. In neutral conditions, the same two signals were observed, plus one small peak at 288.5 eV, attributed to C=O bonds, and finally a shake-up peak at 292.9 eV, attributed to aromatic carbons.[38] These signals are thus generally consistent with the spectral signatures of FAL and its reduction products adsorbed at the surface of the electrode. We note that because of the lower signal-to-noise ratio obtained in acidic conditions, it is probable that the small C=O and aromatic shake-up signals exist but are within the noise of the measurement. To gain insight into the nature of the adsorbed chemicals, the atomic contribution of each of the aforementioned XPS peaks to the entire spectrum have been measured and are displayed in **Figure 6c**. In acidic conditions, we calculated an 80/20 ratio for the C-C/C-H over C-O bond signals. This composition is close to the theoretical composition of 2-MF (83/17) and suggests that the surface of the electrode is mostly covered in reduction products. On the other hand, in neutral conditions, a 79/15/6 distribution for C-C/C-H, C-O and C=O bonds respectively rather suggests a significant coverage of FAL (theoretical distribution of 72/18/9) molecules on the surface of the electrode at the end of the electrolysis. This led us to conclude that FAL is rapidly



https://doi.org/10.26434/chemrxiv-2023-5328j-v2 **ORCID:** https://orcid.org/0000-0003-4367-5502 Content not peer-reviewed by ChemRxiv. **License:** CC BY-NC 4.0

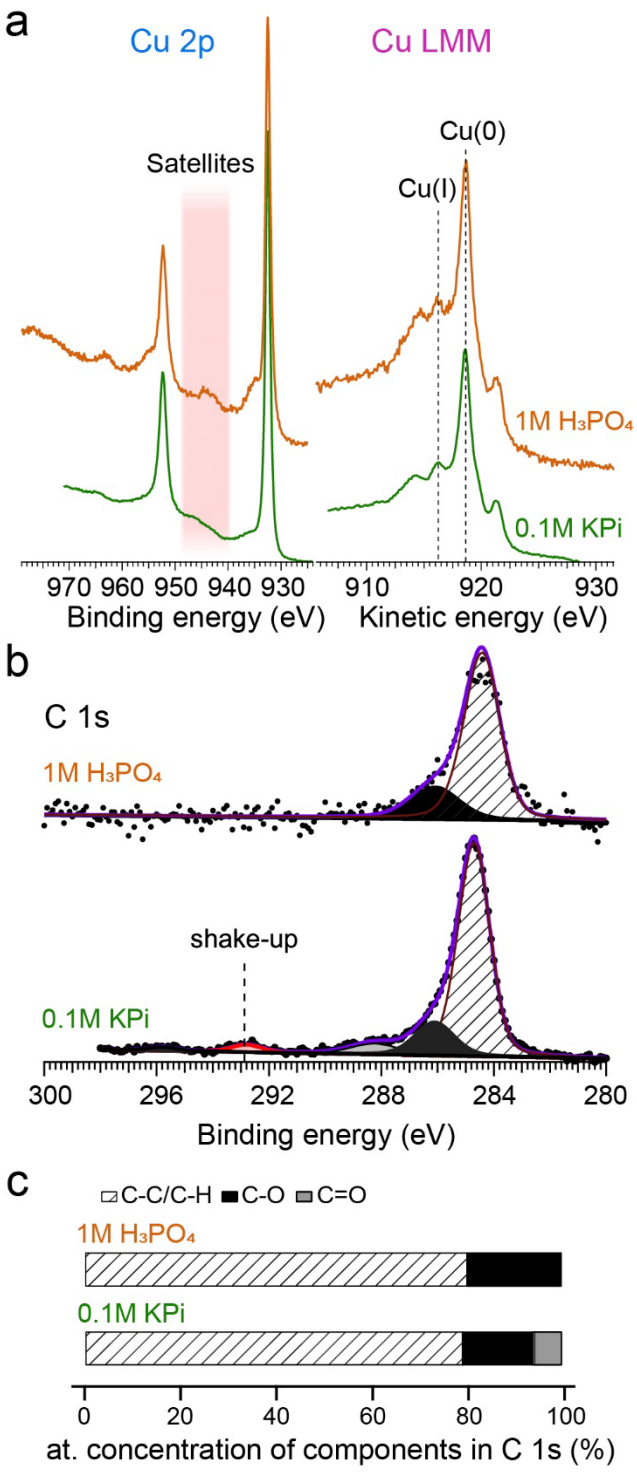


506

507 **Figure 6** a) Cu 2p and Cu LMM XPS spectra measured on structured electrodes under quasi in-
508 situ conditions after 30 min of electrolysis at - 0.5 V vs. RHE in 1M $H_3PO_4$ (orange trace) or 0.1M
509 KPi (green trace) containing 0.01M FAL. b) C 1s spectra measured after 30 min of electrolysis at



https://doi.org/10.26434/chemrxiv-2023-5328j-v2 **ORCID:** https://orcid.org/0000-0003-4367-5502 Content not peer-reviewed by ChemRxiv. **License:** CC BY-NC 4.0

– 0.5 V vs. RHE in 1M $H_3PO_4$ (top graph) or 0.1M KPi (bottom graph) containing 0.01M FAL. c) Atomic percent of C 1s components extracted from spectra displayed in b.

reduced once adsorbed on the surface of the electrode in acidic conditions, making the electrochemical process limited by the desorption of reaction products. On the contrary, FAL is converted more slowly in neutral conditions and tends to accumulate on the surface of the electrode, suggesting the electrochemical process is limited by its conversion. To further approach operating conditions with our spectroscopy measurements, we set out to perform proper in-situ atmospheric pressure XPS (AP-XPS) experiments at the HIPPIE beamline of the MAX IV synchrotron light source in Lund, Sweden.[39] Briefly, it consisted in performing XPS measurements directly at the surface of a working electrode connected to a three-electrode setup immersed in a liquid electrolyte inside an analysis chamber pressurized at 12-15 mbar (see Methods section for more details). Unfortunately, because the structured electrodes were rapidly soaked by the electrolyte, the signals of interest (Cu 2p and C 1s) were masked by the water signal and they could not be analyzed under this configuration. Still, in-situ XPS measurements were performed on copper foil that presented suitable wettability. Moreover, 1M $H_3PO_4$ was chosen as the electrolyte, because of the rapid precipitation of KPi at the surface of the electrode during the acquisition of in-situ XPS data. The CV obtained on the copper electrode inside the XPS chamber is displayed in **Figure 7**. A first series of measurements was conducted in pure 1 M $H_3PO_4$ electrolyte. The Cu 2p XPS spectrum of the electrode surface was measured at several potentials from + 0.2 V to - 0.5 V vs. RHE. The results are shown in **Figure 7c**. They revealed that, while Cu(II) species existed at potentials higher than + 0.1 V vs. RHE, they were progressively reduced to Cu(0) and Cu(I) species when scanning to more negative potentials. The presence of Cu(I) was also confirmed by analysis of the Cu LMM Auger signal (see **Figure S15**). After adding 0.01 M FAL to the electrolyte, the same experiment was conducted, only this time focusing on analyzing the C 1s



https://doi.org/10.26434/chemrxiv-2023-5328j-v2 **ORCID:** https://orcid.org/0000-0003-4367-5502 Content not peer-reviewed by ChemRxiv. **License:** CC BY-NC 4.0

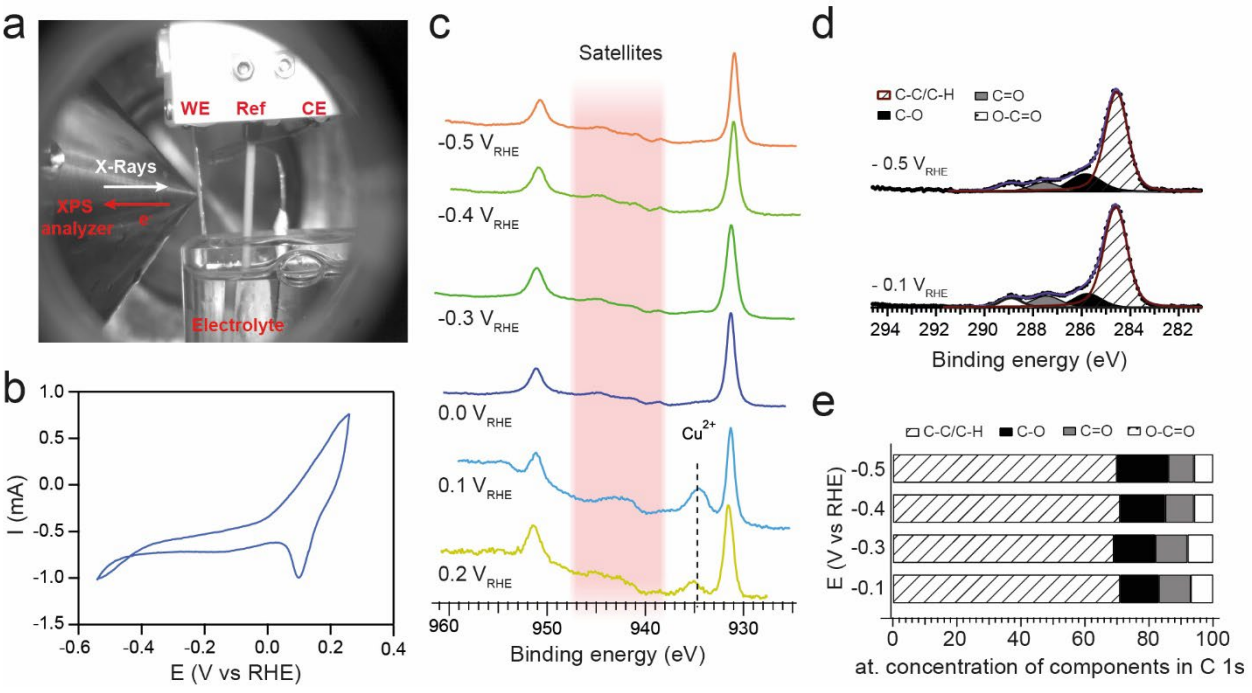


**Figure 7** a) Photograph picture of the experimental three-electrode setup inserted inside the XPS chamber on the HIPPIE beamline at the MAX IV light source facility. b) Cyclic voltammetry acquired with the setup pictured in a, on a copper foil immersed in a 1 M $H_3PO_4$ electrolyte containing 0.01 M of FAL. c) In-situ Cu 2p spectra acquired at different potentials for a copper foil immersed in 1 M $H_3PO_4$. d) In-situ C 1s spectra acquired at – 0.1 V and – 0.5 V vs. RHE at the surface of a copper foil immersed in a 1 M $H_3PO_4$ + 0.01 M FAL electrolyte. e) Atomic percent of C 1s components extracted from in-situ C 1s spectra acquired on copper foil at different potentials in 1 M $H_3PO_4$ + 0.01 M FAL electrolyte.

signal (because the organic layer deposited on the surface of the electrode was masking the Cu 2p signal of the subastrate, it was not possible to monitor both elements at the same time). Quantitative analysis of the C 1s spectra (**Figure 7d-e**) revealed that as the potential was shifted more negatively, the ratio of C-O/C=O increased noticeably between – 0.4 V and – 0.5 V vs. RHE, confirming the reduction of FAL at the surface of the electrode. Interestingly, a peak attributed to O-C=O moieties, absent from the quasi in-situ experiment performed in the lab and reported in **Figure 7**, was identified at all potentials. This was attributed to the oxidation of FAL at the counter-



https://doi.org/10.26434/chemrxiv-2023-5328j-v2 **ORCID:** https://orcid.org/0000-0003-4367-5502 Content not peer-reviewed by ChemRxiv. **License:** CC BY-NC 4.0

electrode and migration to the working electrode inside the undivided electrochemical cell. Indeed, the electrochemical cell employed at the HIPPIE beamline was unseparated, as opposed to the one employed in the experiment described in **Figure 6.** While the existence of this crossover affected the analysis of the organic layer, it still supported the observations made with the quasi in-situ experiment performed in the laboratory on the state of Cu and C under operating conditions. This demonstrated the ability of using AP-XPS for analyzing both the oxidation state of the electrode and the composition of the adsorbed organic layer at its surface under quasi-operating conditions, providing insight into the catalytic process at the molecular level.

## Conclusion

The self-templated copper electrocatalyst presented in this work exhibited improved activity and selectivity compared to unstructured copper foil. More specifically, studying the influence of temperature and applied potential on the outcome of the electrocatalytic process allowed to identify experimental conditions in which (i) FOH could be selectively produced from FAL in a neutral electrolyte with a 100% FE at unprecedently low overpotential and (ii) either FOH or 2-MF could be selectively produced from FAL in acidic condition, at similarly low overpotentials, albeit with strong HER competition. The existence of this optimum for FAL illustrates the importance of the combined influence of these two driving forces (voltage and temperature) on the selectivity of complex electrocatalytic processes. Quasi in-situ and in-situ photoelectron spectroscopy was further found to be an insightful tool to shed light on the mechanism of this process, as the analysis of Cu 2p and C 1s signal revealed the resilience of Cu (I) species under operating conditions, as well as a difference in the oxidation state of the organic layer adsorbed at the surface of the electrode, pointing towards differences in the limiting step of electrocatalytic mechanisms between neutral and acidic conditions. While this work demonstrates the benefits of structured Cu



https://doi.org/10.26434/chemrxiv-2023-5328j-v2 **ORCID:** https://orcid.org/0000-0003-4367-5502 Content not peer-reviewed by ChemRxiv. **License:** CC BY-NC 4.0

electrodes over Cu foil in terms of activity and selectivity, important competition from the HER remained in acidic conditions. Experimental and theoretical investigations as well as cell design optimization are under way to understand how to further improve the performance of this system.

## AUTHOR INFORMATION

Corresponding Author

*mathieu.prevot@ircelyon.univ-lyon1.fr

Author Contributions

The manuscript was written through contributions of all authors. All authors have given approval to the final version of the manuscript.

Notes

The authors declare no competing financial interest.

## ASSOCIATED CONTENT

**Supporting Information**. The following files are available free of charge.
A PDF containing illustrations of the methods employed in the study, additional SEM data, additional cyclic voltammetry and chronoamperometry data, complementary activity and selectivity data obtained on structured Cu and Cu foil, activation energy measurements, details on the detection and quantification of dissolved products by HPLC and NMR, additional XPS data and a literature survey of state-of-the-art electrocatalysts for the reduction of furfural.

## ACKNOWLEDGMENT



https://doi.org/10.26434/chemrxiv-2023-5328j-v2 **ORCID:** https://orcid.org/0000-0003-4367-5502 Content not peer-reviewed by ChemRxiv. **License:** CC BY-NC 4.0

We thank the following funding sources for this project: the Marie Skłodowska-Curie action SOLBIOCHEM (project n° 896901), the French National Agency for Research (ANR) project MEGOPE (ANR-22-CE29-0015) and the European Innovation Council (EIC) Pathfinder Project ELOBIO (grant agreement n° 101070856).

We acknowledge MAX IV Laboratory for time on Beamline HIPPIE under Proposal 20210958. Research conducted at MAX IV, a Swedish national user facility, is supported by the Swedish Research council under contract 2018-07152, the Swedish Governmental Agency for Innovation Systems under contract 2018-04969, and Formas under contract 2019-02496.

We thank the Technological Center on Microstructures of the University of Lyon for access to the Scanning Electron Microscope through their microscopy platform. We also wish to thank the platform IRCATECH platform for acquiring the XRD data shown in this paper.

## REFERENCES

(1) Dahmen, N.; Lewandowski, I.; Zibek, S.; Weidtmann, A. Integrated Lignocellulosic Value Chains in a Growing Bioeconomy: Status Quo and Perspectives. *GCB Bioenergy* **2019**, *11* (1), 107–117. https://doi.org/10.1111/gcbb.12586.

(2) Mariscal, R.; Maireles-Torres, P.; Ojeda, M.; Sádaba, I.; Granados, M. L. Furfural: A Renewable and Versatile Platform Molecule for the Synthesis of Chemicals and Fuels. *Energy & Environmental Science* **2016**, *9* (4), 1144–1189. https://doi.org/10.1039/C5EE02666K.

(3) Tang, C.; Zheng, Y.; Jaroniec, M.; Qiao, S.-Z. Electrocatalytic Refinery for Sustainable Production of Fuels and Chemicals. *Angewandte Chemie International Edition* **2021**, *60* (36), 19572–19590. https://doi.org/10.1002/anie.202101522.

(4) Lucas, F. W. S.; Grim, R. G.; Tacey, S. A.; Downes, C. A.; Hasse, J.; Roman, A. M.; Farberow, C. A.; Schaidle, J. A.; Holewinski, A. Electrochemical Routes for the Valorization of Biomass-Derived Feedstocks: From Chemistry to Application. *ACS Energy Lett.* **2021**, *6* (4), 1205–1270. https://doi.org/10.1021/acsenergylett.0c02692.

(5) Shang, X.; Yang, Y.; Sun, Y. Electrohydrodimerization of Biomass-Derived Furfural Generates a Jet Fuel Precursor. *Green Chem.* **2020**, *22* (16), 5395–5401. https://doi.org/10.1039/D0GC01720E.

(6) Temnikova, M.; Medvedev, J.; Medvedeva, X.; Delva, N. H.; Khairullina, E.; Krivoshapkina, E.; Klinkova, A. Electrochemical Hydrodimerization of Furfural in Organic Media as an



https://doi.org/10.26434/chemrxiv-2023-5328j-v2 **ORCID:** https://orcid.org/0000-0003-4367-5502 Content not peer-reviewed by ChemRxiv. **License:** CC BY-NC 4.0

Efficient Route to Jet Fuel Precursor. *ChemElectroChem* **2023**, *10* (2), e202200865. https://doi.org/10.1002/celc.202200865.
(7) Liu, S.; Mukadam, Z.; Scott, S. B.; Sarma, S. C.; Titirici, M.-M.; Chan, K.; Govindarajan, N.; Stephens, I. E. L.; Kastlunger, G. Unraveling the Reaction Mechanisms for Furfural Electroreduction on Copper. *EES. Catal.* **2023**, *1* (4), 539–551. https://doi.org/10.1039/D3EY00040K.
(8) Green, S. K.; Lee, J.; Kim, H. J.; Tompsett, G. A.; Kim, W. B.; Huber, G. W. The Electrocatalytic Hydrogenation of Furanic Compounds in a Continuous Electrocatalytic Membrane Reactor. *Green Chem.* **2013**, *15* (7), 1869–1879. https://doi.org/10.1039/C3GC00090G.
(9) Chadderdon, X. H.; Chadderdon, D. J.; Matthiesen, J. E.; Qiu, Y.; Carraher, J. M.; Tessonnier, J.-P.; Li, W. Mechanisms of Furfural Reduction on Metal Electrodes: Distinguishing Pathways for Selective Hydrogenation of Bioderived Oxygenates. *J. Am. Chem. Soc.* **2017**, *139* (40), 14120–14128. https://doi.org/10.1021/jacs.7b06331.
(10) Albert, W. C.; Lowy, A. The Electrochemical Reduction of Furfural. *Trans. Electrochem. Soc.* **1939**, *75* (1), 367. https://doi.org/10.1149/1.3498392.
(11) Kwon, Y.; Schouten, K. J. P.; van der Waal, J. C.; de Jong, E.; Koper, M. T. M. Electrocatalytic Conversion of Furanic Compounds. *ACS Catal.* **2016**, *6* (10), 6704–6717. https://doi.org/10.1021/acscatal.6b01861.
(12) Li, K.; Sun, Y. Electrocatalytic Upgrading of Biomass-Derived Intermediate Compounds to Value-Added Products. *Chemistry – A European Journal* **2018**, *24* (69), 18258–18270. https://doi.org/10.1002/chem.201803319.
(13) May, A. S.; Biddinger, E. J. Strategies to Control Electrochemical Hydrogenation and Hydrogenolysis of Furfural and Minimize Undesired Side Reactions. *ACS Catal.* **2020**, *10* (5), 3212–3221. https://doi.org/10.1021/acscatal.9b05531.
(14) Wen, H.; Zhang, W.; Fan, Z.; Chen, Z. Recent Advances in Furfural Reduction via Electro- And Photocatalysis: From Mechanism to Catalyst Design. *ACS Catal.* **2023**, 15263–15289. https://doi.org/10.1021/acscatal.3c04372.
(15) Chamoulaud, G.; Floner, D.; Moinet, C.; Lamy, C.; Belgsir, E. M. Biomass Conversion II: Simultaneous Electrosyntheses of Furoic Acid and Furfuryl Alcohol on Modified Graphite Felt Electrodes. *Electrochimica Acta* **2001**, *46* (18), 2757–2760. https://doi.org/10.1016/S0013-4686(01)00507-2.
(16) Parpot, P.; Bettencourt, A. P.; Chamoulaud, G.; Kokoh, K. B.; Belgsir, E. M. Electrochemical Investigations of the Oxidation–Reduction of Furfural in Aqueous Medium: Application to Electrosynthesis. *Electrochimica Acta* **2004**, *49* (3), 397–403. https://doi.org/10.1016/j.electacta.2003.08.021.
(17) Li, Z.; Kelkar, S.; Lam, C. H.; Luczek, K.; Jackson, J. E.; Miller, D. J.; Saffron, C. M. Aqueous Electrocatalytic Hydrogenation of Furfural Using a Sacrificial Anode. *Electrochimica Acta* **2012**, *64*, 87–93. https://doi.org/10.1016/j.electacta.2011.12.105.
(18) zhao, B.; Chen, M.; Guo, Q.; Fu, Y. Electrocatalytic Hydrogenation of Furfural to Furfuryl Alcohol Using Platinum Supported on Activated Carbon Fibers. *Electrochimica Acta* **2014**, *135*, 139–146. https://doi.org/10.1016/j.electacta.2014.04.164.
(19) Nilges, P.; Schröder, U. Electrochemistry for Biofuel Generation: Production of Furans by Electrocatalytic Hydrogenation of Furfurals. *Energy Environ. Sci.* **2013**, *6* (10), 2925–2931. https://doi.org/10.1039/C3EE41857J.



https://doi.org/10.26434/chemrxiv-2023-5328j-v2 **ORCID:** https://orcid.org/0000-0003-4367-5502 Content not peer-reviewed by ChemRxiv. **License:** CC BY-NC 4.0

(20) Jung, S.; Biddinger, E. J. Electrocatalytic Hydrogenation and Hydrogenolysis of Furfural and the Impact of Homogeneous Side Reactions of Furanic Compounds in Acidic Electrolytes. *ACS Sustainable Chem. Eng.* **2016**, *4* (12), 6500–6508. https://doi.org/10.1021/acssuschemeng.6b01314.
(21) Jung, S.; Biddinger, E. J. Controlling Competitive Side Reactions in the Electrochemical Upgrading of Furfural to Biofuel. *Energy Technology* **2018**, *6* (7), 1370–1379. https://doi.org/10.1002/ente.201800216.
(22) Jung, S.; Karaiskakis, A. N.; Biddinger, E. J. Enhanced Activity for Electrochemical Hydrogenation and Hydrogenolysis of Furfural to Biofuel Using Electrodeposited Cu Catalysts. *Catalysis Today* **2019**, *323*, 26–34. https://doi.org/10.1016/j.cattod.2018.09.011.
(23) Anibal, J.; Xu, B. Electroreductive C–C Coupling of Furfural and Benzaldehyde on Cu and Pb Surfaces. *ACS Catal.* **2020**, *10* (19), 11643–11653. https://doi.org/10.1021/acscatal.0c03110.
(24) Zhou, P.; Chen, Y.; Luan, P.; Zhang, X.; Yuan, Z.; Guo, S.-X.; Gu, Q.; Johannessen, B.; Mollah, M.; Chaffee, A. L.; Turner, D. R.; Zhang, J. Selective Electrochemical Hydrogenation of Furfural to 2-Methylfuran over a Single Atom Cu Catalyst under Mild pH Conditions. *Green Chem.* **2021**, *23* (8), 3028–3038. https://doi.org/10.1039/D0GC03999C.
(25) Zhou, P.; Li, L.; Mosali, V. S. S.; Chen, Y.; Luan, P.; Gu, Q.; Turner, D. R.; Huang, L.; Zhang, J. Electrochemical Hydrogenation of Furfural in Aqueous Acetic Acid Media with Enhanced 2-Methylfuran Selectivity Using CuPd Bimetallic Catalysts. *Angewandte Chemie* **2022**, *134* (13), e202117809. https://doi.org/10.1002/ange.202117809.
(26) Xia, Z.; Li, Y.; Wu, J.; Huang, Y.-C.; Zhao, W.; Lu, Y.; Pan, Y.; Yue, X.; Wang, Y.; Dong, C.-L.; Wang, S.; Zou, Y. Promoting the Electrochemical Hydrogenation of Furfural by Synergistic Cu0−Cu+ Active Sites. *Sci. China Chem.* **2022**, *65* (12), 2588–2595. https://doi.org/10.1007/s11426-022-1407-0.
(27) Cui, Y.; Wang, Z.; Li, S. Electrocatalytic Reduction of Furfural for Selective Preparation of 2-Methylfuran over a Trace Ni Assisted Cu Catalyst. *Catal. Sci. Technol.* **2023**, *13* (6), 1846–1854. https://doi.org/10.1039/D3CY00126A.
(28) Cao, Y.; Noël, T. Efficient Electrocatalytic Reduction of Furfural to Furfuryl Alcohol in a Microchannel Flow Reactor. *Org. Process Res. Dev.* **2019**, *23* (3), 403–408. https://doi.org/10.1021/acs.oprd.8b00428.
(29) Li, Y.; Jia, W.-Z.; Song, Y.-Y.; Xia, X.-H. Superhydrophobicity of 3D Porous Copper Films Prepared Using the Hydrogen Bubble Dynamic Template. *Chem. Mater.* **2007**, *19* (23), 5758–5764. https://doi.org/10.1021/cm071738j.
(30) Plowman, B. J.; Jones, L. A.; Bhargava, S. K. Building with Bubbles: The Formation of High Surface Area Honeycomb-like Films via Hydrogen Bubble Templated Electrodeposition. *Chem. Commun.* **2015**, *51* (21), 4331–4346. https://doi.org/10.1039/C4CC06638C.
(31) Maheu, C.; Cardenas, L.; Puzenat, E.; Afanasiev, P.; Geantet, C. UPS and UV Spectroscopies Combined to Position the Energy Levels of TiO2 Anatase and Rutile Nanopowders. *Phys. Chem. Chem. Phys.* **2018**, *20* (40), 25629–25637. https://doi.org/10.1039/C8CP04614J.
(32) Pérez Sánchez, M.; Barrera, M.; González, S.; Souto, R. M.; Salvarezza, R. C.; Arvia, A. J. Electrochemical Behaviour of Copper in Aqueous Moderate Alkaline Media, Containing Sodium Carbonate and Bicarbonate, and Sodium Perchlorate. *Electrochimica Acta* **1990**, *35* (9), 1337–1343. https://doi.org/10.1016/0013-4686(90)85004-7.



https://doi.org/10.26434/chemrxiv-2023-5328j-v2 **ORCID:** https://orcid.org/0000-0003-4367-5502 Content not peer-reviewed by ChemRxiv. **License:** CC BY-NC 4.0

(33) Long, J.; Zhao, W.; Xu, Y.; Wu, W.; Fang, C.; Li, H.; Yang, S. Low-Temperature Catalytic Hydrogenation of Bio-Based Furfural and Relevant Aldehydes Using Cesium Carbonate and Hydrosiloxane. *RSC Advances* **2019**, *9* (6), 3063–3071. https://doi.org/10.1039/C8RA08616H.
(34) Durndell, L. J.; Parlett, C. M. A.; Hondow, N. S.; Isaacs, M. A.; Wilson, K.; Lee, A. F. Selectivity Control in Pt-Catalyzed Cinnamaldehyde Hydrogenation. *Sci Rep* **2015**, *5* (1), 9425. https://doi.org/10.1038/srep09425.
(35) An, W.; Men, Y.; Wang, J. Comparative Study on Hydrogenation of Propanal on Ni(111) and Cu(111) from Density Functional Theory. *Applied Surface Science* **2017**, *394*, 333–339. https://doi.org/10.1016/j.apsusc.2016.10.064.
(36) Song, Y.; Sanyal, U.; Pangotra, D.; Holladay, J. D.; Camaioni, D. M.; Gutiérrez, O. Y.; Lercher, J. A. Hydrogenation of Benzaldehyde via Electrocatalysis and Thermal Catalysis on Carbon-Supported Metals. *Journal of Catalysis* **2018**, *359*, 68–75. https://doi.org/10.1016/j.jcat.2017.12.026.
(37) May, A. S.; Watt, S. M.; Biddinger, E. J. Kinetics of Furfural Electrochemical Hydrogenation and Hydrogenolysis in Acidic Media on Copper. *React. Chem. Eng.* **2021**, *6* (11), 2075–2086. https://doi.org/10.1039/D1RE00216C.
(38) Gengenbach, T. R.; Major, G. H.; Linford, M. R.; Easton, C. D. Practical Guides for X-Ray Photoelectron Spectroscopy (XPS): Interpreting the Carbon 1s Spectrum. *Journal of Vacuum Science & Technology A: Vacuum, Surfaces, and Films* **2021**, *39* (1), 013204. https://doi.org/10.1116/6.0000682.
(39) Zhu, S.; Scardamaglia, M.; Kundsen, J.; Sankari, R.; Tarawneh, H.; Temperton, R.; Pickworth, L.; Cavalca, F.; Wang, C.; Tissot, H.; Weissenrieder, J.; Hagman, B.; Gustafson, J.; Kaya, S.; Lindgren, F.; Källquist, I.; Maibach, J.; Hahlin, M.; Boix, V.; Gallo, T.; Rehman, F.; D'Acunto, G.; Schnadt, J.; Shavorskiy, A. HIPPIE: A New Platform for Ambient-Pressure X-Ray Photoelectron Spectroscopy at the MAX IV Laboratory. *J Synchrotron Rad* **2021**, *28* (2), 624–636. https://doi.org/10.1107/S160057752100103X.

**Graphical abstract:**

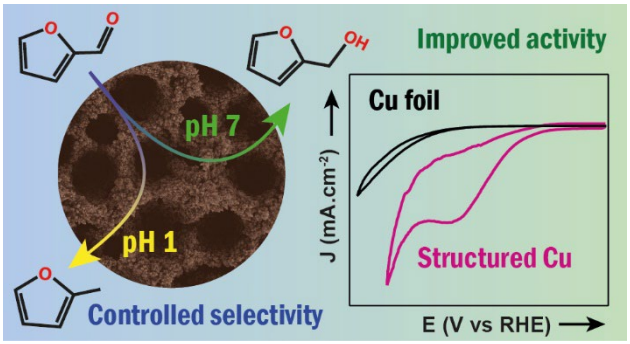




https://doi.org/10.26434/chemrxiv-2023-5328j-v2 **ORCID:** https://orcid.org/0000-0003-4367-5502 Content not peer-reviewed by ChemRxiv. **License:** CC BY-NC 4.0